Nanoscale

PAPER

View Article Online
View Journal | View Issue

Cite this: *Nanoscale*, 2025, **17**, 2608

Influence of zinc oxide nanoparticles on the carbon accumulation on silver exposed to carbon dioxide hydrogenation reaction conditions†

Paul Maurice Leidinger, *‡[a] Mirco Panighel, §[c] Vitaly L. Sushkevich, [a] Paolo Piseri, [d,e] Alessandro Podestà, [d] Jeroen A. van Bokhoven [a,b] and Luca Artiglia *[a]

Received 13th September 2024,
Accepted 10th January 2025

DOI: 10.1039/d4nr03766a

rsc.li/nanoscale

The strong influence of surface adsorbates on the morphology of a catalyst is exemplified by studying a silver surface with and without deposited zinc oxide nanoparticles upon exposure to reaction gases used for carbon dioxide hydrogenation. Ambient pressure X-ray photoelectron spectroscopy and scanning tunneling microscopy measurements indicate accumulation of carbon deposits on the catalyst surface at 200 °C. While oxygen-free carbon species observed on pure silver show a strong interaction and decorate the atomic steps on the catalyst surface, this decoration is not observed for the oxygen-containing species observed on the silver surface with additional zinc oxide nanoparticles. Annealing the sample to temperatures above 350 °C removes the contaminants by hydrogenation to methane.

Introduction

The activity of heterogeneous catalysts is majorly defined by their topmost atomic layers. Surface sites, such as step edges, corner sites and kinks are known to be key elements for many catalytic reactions.[1,2] As the surface composition of a material can strongly differ between reaction conditions and *ex situ* analysis, a key challenge is to investigate those catalytically-relevant interfaces *in situ*, while exposed to the reactive environment.[3]

While there are several short-lived species (reaction intermediates) crucial for the understanding of a catalyst's selectivity and activity,[4–6] there are often also passive deposits that influence the catalytic activity of a material. These accumulating species can for example block active sites, deactivate and poison the material over time,[7,8] but also change the surface structure of the catalytic material.[9,10] Catalyst regeneration cycles often consist of annealing cycles in oxygen to burn contaminations,[11] while for reducing reactions also the gasification in hydrogen is applied.[12]

Previous studies have shown that silver-based catalysts show a high selectivity towards methanol for the carbon dioxide hydrogenation reaction (eqn (1)).[13] The reverse water–gas-shift (RWGS) reaction (eqn (2)), a side reaction that yields carbon monoxide (CO) and water, can be suppressed by carefully tuning the catalyst composition.

$$CO_2 + 3H_2 \rightarrow H_3COH + H_2O \quad (1)$$

$$CO_2 + H_2 \rightarrow CO + H_2O \quad (2)$$

Within this framework, a surface sensitive method like X-ray photoelectron spectroscopy (XPS), carried out under ambient pressure (AP) conditions (mbar pressure range),[3] may provide important information not only about the formation of reaction intermediates, but also about the activity loss due to site deactivation through carbon accumulation/poisoning. However, while the formation of methanol from carbon dioxide hydrogenation is thermodynamically unfavourable in the mbar range,[14] the RWGS reaction does not similarly suffer from a pressure gap and can be probed under conditions (temperature and pressure) achievable by AP-XPS.[15]

[a]*Center for Energy and Environmental Sciences, Paul Scherrer Institute, Forschungsstrasse 111, 5232 Villigen, Switzerland.*
E-mail: paul.leidinger@inano.au.dk
[b]*Institute for Chemical and Bioengineering, ETH Zurich, Vladimir-Prelog-Weg 1, 8093 Zurich, Switzerland*
[c]*CNR - Istituto Officina dei Materiali (IOM), Trieste, Laboratorio TASC, Strada Statale 14, km 163.5, 34149 Basovizza, Italy*
[d]*Dipartimento di Fisica, Università degli Studi di Milano, Via Celoria 16, 20133 Milan, Italy*
[e]*Centro Interdisciplinare Materiali e Interfacce Nanostrutturati (CIMAINA), Università degli Studi di Milano, Via Celoria 16, 20133 Milan, Italy*

†Electronic supplementary information (ESI) available. See DOI: https://doi.org/10.1039/d4nr03766a

‡Present address: Interdisciplinary Nanoscience Center (iNANO), Aarhus University, 8000 Aarhus C, Denmark.

§Present address: Scanning Probe Microscopy Laboratory, Department of Physics and Materials Science, University of Luxembourg, Luxembourg City L-1511, Luxembourg.

In this work, we exemplarily show that such accumulating species can have a strong effect on the surface morphology of a catalyst. We analyze the impact of accumulating carbon-based contaminations on model silver foils under carbon dioxide hydrogenation conditions by AP-XPS and scanning tunneling microscopy (STM). It is known from studies carried out on complex catalysts for carbon dioxide hydrogenation, such as $Cu/ZnO/Al_2O_3$, that the transition metal dissociatively adsorbs hydrogen. Carbon dioxide is mostly adsorbed on the ZnO/Al_2O_3 phase or its interface with copper.[14,16] Based on these observations, we add zinc oxide nanoparticles to a silver substrate, increasing the complexity of the catalyst and getting closer to the structure of industrially-used bifunctional catalysts. The goal is to investigate the stability and evolution of carbon contaminations in the presence of the oxide. The results show that the silver surface structure is highly dependent on the reaction conditions. Oxygen-free carbon species tend to decorate and pin silver step edges, while oxygen-containing carbon species, observed in the presence of zinc oxide nanoparticles, show less interaction with the step edges and do not accumulate on specific surface sites. These results shed light on the mutual influence between the metal and the oxide in carbon dioxide hydrogenation catalysts.

Experimental results

Silver foil

Polycrystalline silver foil was used as a model system to study the carbon dioxide hydrogenation reaction, where silver is active for the hydrogen dissociation.[17,18] The silver foil was exposed to a $H_2 + CO_2$ mixture (3 : 1 ratio) at a total pressure of 0.2 mbar while recording *in situ* photoemission spectra. Fig. 1(a) shows the evolution of the C 1s signal over 120 min with the substrate held at 250 °C after cooling it down from 350 °C (first spectrum in waterfall plot, lower spectrum in Fig. 1b). The *in situ* C 1s spectrum acquired at 350 °C shows no features, except for a signal centered at approx. 293 eV, assigned to gas phase carbon dioxide. At 250 °C a signal at 284.5 eV appears which increases in intensity over time. A less intense component at 285.9 eV also appears during the exposure at 250 °C. During this time, the O 1s signal shows no significant increase in intensity (see Fig. S1†). Fig. 1c shows the C 1s signal evolution (both surface carbon species at 284.5 + 285.9 eV) with time at different temperatures in monolayer equivalents (see Table S1 and Fig. S2† for calculation details). The initial carbon accumulation rate depends on the substrate temperature, dropping from the maximum of roughly $8.0\%_{ML}$ min^{-1} at 200 °C to $2.5\%_{ML}$ min^{-1} at 300 °C (Fig. S3†). At 350 °C, the surface shows no more accumulation of carbon-based species. A saturation of the accumulated carbon occurs after 60–120 min of exposure depending on the temperature, with a maximum observed coverage of roughly 1 ML. Continuous red lines in the plot in Fig. 1c show the fits by an asymptotic regression model. The carbon accumulation in inert nitrogen gas and pure carbon dioxide (control experiments) occurs to significantly lower extent (see Fig. S4 and S5†).

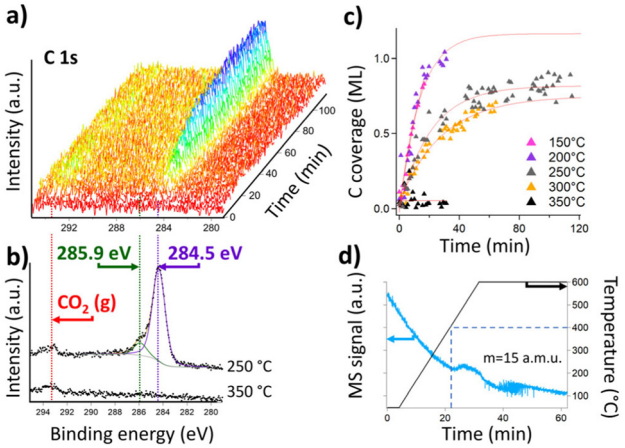

Fig. 1 Evolution of the surface composition of a silver foil exposed to carbon dioxide-hydrogenation conditions, measured by AP-XPS and hydrogen temperature-programmed reaction (H_2-TPR). (a) Evolution of the C 1s signal (photon energy 437 eV) of a silver foil exposed to 0.2 mbar $H_2 + CO_2$ mixture at 250 °C for 120 min. (b) Individual C 1s spectra acquired at 350 °C (bottom) show no C accumulation (averaged spectra between 0–30 min acquisition) and 250 °C (top) show significant C accumulation (averaged spectra between 90–120 min acquisition). This spectrum is fitted with 2 components at 284.5 eV (assigned to C–C and C–H species) and 285.9 eV (assigned to impurity-induced accumulation). The carbon dioxide gas phase signal can be detected around 293 eV. (c) Quantification of the accumulated surface carbon species (284.5 + 285.9 eV) for different temperatures. The red lines represent fittings using an asymptotic regression model. (d) Mass spectrometry signal for mass 15 a.m.u. of a silver powder sample pre-exposed to $H_2 + CO_2$ at 200 °C for 30 min and subsequently heated in 1 bar hydrogen up to 600 °C. Mass 15 a.m.u. is identified as a fragment of CH_4.

To gain insights into the effect of the accumulating species on the morphology of the sample, STM measurements were performed on a silver film evaporated on cleaved mica substrate exposed to the $H_2 + CO_2$ reaction mixture (1 mbar, 3 : 1 ratio) at high-temperature conditions (60 min 350 °C + 5 min 375 °C, no C 1s accumulation observed by XPS) and low-temperature conditions (60 min 200 °C, relevant C 1s accumulation observed by XPS). Representative images of both samples are shown in Fig. 2 and S6–S8.† Upon high-temperature exposure, the sample shows mostly flat regions without defined crystallinity or atomic steps over ranges of up to 50 nm (Fig. S7a†). Scarcely, very mobile terraces can be found, as shown in Fig. S6.† The sample exposed to the reaction mixture at 200 °C (Fig. 2b and S8†) on the other hand shows a large number of steps. Many of these atomic steps show a defined edge together with a protrusion in height of up to 0.15 nm, although also steps without these clear protrusions can be found in a minority of the identified steps (see Fig. S8†). The flat surface without edge protrusions can be re-established after the subsequent annealing treatment, in the same way as accumulated carbon species are removed upon the high-temperature exposure, as observed by *in situ* AP-XPS (Fig. 1).

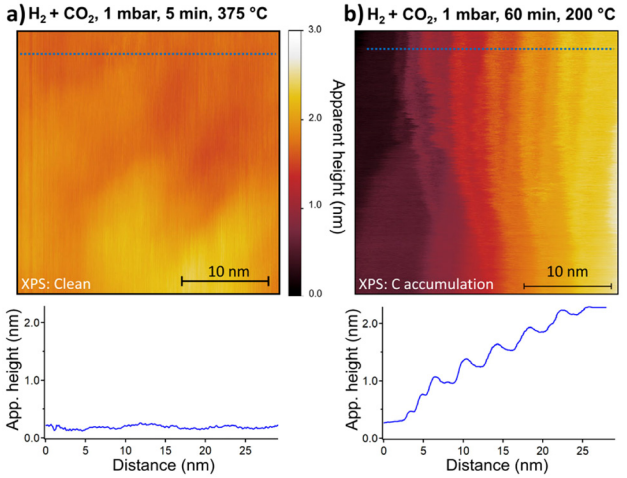

Fig. 2 STM images of the silver foil after exposure to CO_2 hydrogenation gas mixtures. (a) Silver film (evaporated on Mica substrate) exposed to 1 mbar H_2 + CO_2 atmosphere for 60 min at 350 °C and additional 5 min at 375 °C. The image shows slight protrusions of 1–2 Å over the image size of 30 nm, caused by the lack of crystallinity of the measured sample. The height profile shown below is indicated with a blue dotted line in the image. Further images in Fig. S6 and S7.† (b) Silver foil exposed to 1 mbar H_2 + CO_2 atmosphere for 60 min at 200 °C. The image shows a strongly stepped surface. Protrusions of up to 0.15 nm at the step edges indicate their decoration with a surface species. Further images in Fig. S8.†

To understand the nature of the accumulating species and its reactivity, hydrogen temperature-programmed reaction (H_2-TPR) was performed on a silver powder. The higher surface area of the powder increases the signal of desorbed molecules, making such an experiment possible. The powder was treated in H_2 + CO_2 (3 : 1 ratio, 1 bar, 200 °C) for 30 min to accumulate carbon species and subsequently heated in 1 bar hydrogen up to 600 °C while recording the gas stream using a mass spectrometer (MS). The MS trace shows the appearance and gradual development of a signal for mass 15 a.m.u., starting at about 400 °C. This can be assigned to the CH_3 fragment of methane, excluding oxygen-containing carbon molecules. Further mass traces are shown in Fig. S9.† Besides 15 a.m.u., the only signals detected are 16 a.m.u., which can be assigned to both water and methane, 17 and 18 a.m.u, which are assigned to water. Upon normalization to the fragmentation pattern of water (Fig. S9c†), the 17 and 18 a.m.u. signals superimpose well, whereas 16 a.m.u. has a larger area that further proves the formation of methane.

Silver foil with zinc oxide nanoparticles

To analyze the influence of the presence of oxide on the accumulation of contaminants and the surface morphology, zinc oxide nanoparticles were deposited on the Ag/mica film. The nanoparticle size shows a distribution centered at 5 nm with a standard deviation of 3 nm, see Fig. S10† for a representative atomic force microscopy (AFM) image and statistical particle size analysis. As the pure silver film, the sample was exposed to a 1 mbar H_2 + CO_2 mixture (3 : 1 ratio) at high-temperature (60 min at 350 °C + 5 min at 375 °C) and low-temperature (60 min at 200 °C) conditions. Representative STM images are shown in Fig. 3 and Fig. S11–S14.† The images displayed in Fig. 3a and b show a large particle in the lower right corner, attributed to zinc oxide. In both cases the silver substrate is mainly flat and without a defined crystalline surface. Few steps in the film can be detected, which appear fringed, with no defined step line. In contrast to the sample without any zinc oxide nanoparticles, no accumulation of surface species (protrusions) at the step edges can be observed, and no increased amount of step edges is found in the sample exposed to the reactive mixture at 200 °C. Note that the inherent width of the STM tip will broaden very confined surface features such as the nanoparticles. Therefore, the measured apparent height (2–4 nm) better indicates also the width of the zinc oxide nanoparticles, assuming a round shape.

High surface area ZnO/Ag catalyst

The interplay between silver and zinc oxide was investigated spectroscopically by AP-XPS using a high surface area ZnO/Ag catalyst, used to simulate the silver foil decorated with zinc oxide nanoparticles described above. The details of the synthesis and characterization of this material can be found in a different study.[13] In situ AP-XPS measurements (Fig. 4a–c) were performed by first exposing the catalyst at 450 °C to 1 mbar oxygen to achieve a carbon-free C 1s spectrum (first spectrum in Fig. 4a waterfall plot). After this, the gas composition was switched to a 0.2 mbar H_2 + CO_2 atmosphere (3 : 1 ratio) at a temperature of 250 °C. The gas phase signal of carbon dioxide (around 293 eV) immediately appears in the C

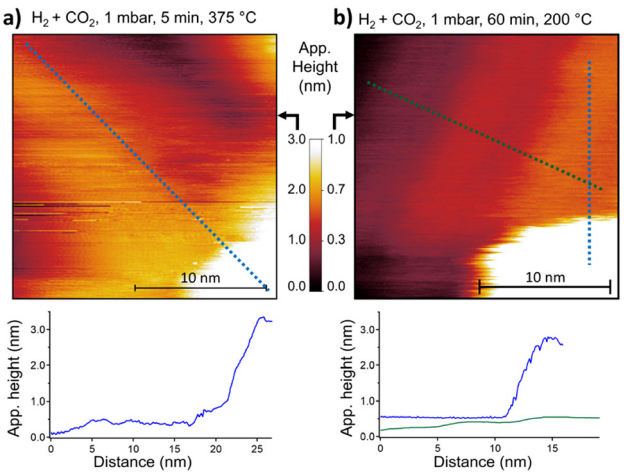

Fig. 3 STM images of the silver foil with zinc oxide nanoparticles (top) and representative height profiles (bottom) after exposure to CO_2 hydrogenation gas mixtures. (a) 1 mbar H_2 + CO_2 atmosphere at 350 °C for 60 min with an additional 5 min at 375 °C. A protrusion in the lower right corner indicates a zinc oxide nanoparticle. Apart from this, the surface shows no defined structure. Further images in Fig. S11.† (b) 1 mbar H_2 + CO_2 atmosphere at 200 °C for 60 min. A zinc oxide nanoparticle is present in the lower right corner. The silver surface shows two diffuse step edges, no edge decoration or other adsorbates can be identified. Further images in Fig. S12–S14.†

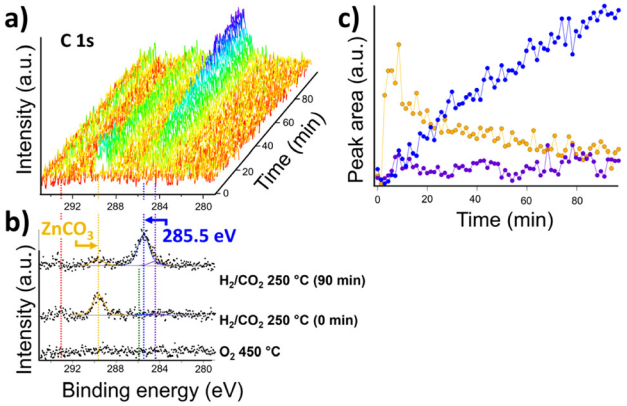

Fig. 4 Elemental analysis of the ZnO/Ag high surface area catalyst exposed to carbon dioxide hydrogenation conditions (H_2 + CO_2) at 0.2 mbar and 250 °C. (a) AP-XPS C 1s spectra arranged in a waterfall-plot to show the evolution of C species on ZnO/Ag at 250 °C in 0.2 mbar H_2 + CO_2 over 90 min. After switching from the clean surface (450 °C, 0.2 mbar O_2), a component at 289.7 eV immediately appears and then reduces and vanishes almost completely over the course of 90 min. Simultaneously, a new peak at 285.5 eV develops. The component at 284.5 eV is observed only very faintly. (b) Representative C 1s spectra of the clean sample (bottom), directly after switching to reaction conditions (middle) and after 90 min of exposure (top). (c) Temporal evolution of the peak area of the species observed at 284.5 eV (purple), 285.5 eV (blue) and 289.7 eV (orange) during exposure to 0.2 mbar H_2 + CO_2 at 250 °C.

1s spectrum, together with a second peak centered at 289.7 eV. Within the first spectra (0–4 min), a carbon signal at lower binding energy is not present, then a peak centered at 285.5 eV appears and its intensity increases over the 90 min of measurement time. This peak is shifted by 1 eV compared to the main species accumulating on the bare silver foil. Within the same timespan, the photoemission signal at 289.7 eV almost completely vanishes, as also displayed in the plot of the relative C 1s signals in Fig. 4c. The O 1s spectrum under reaction conditions is characterized by several overlapping signal contributions from the zinc oxide material and surface species.[13]

Discussion

The C 1s peak appearing at a binding energy of 284.5 eV (Fig. 1a) on the clean silver foil is assigned to oxygen-free carbon species (C–C, C=C and C–H bonds),[19,20] which is also confirmed by the lack of increase in the O 1s signal (Fig. S1†). Fig. 1c shows that the C 1s peak area converges to a "saturation" value corresponding to approximately 1 monolayer. The self-terminating accumulation indicates that specific surface sites are required for the adsorption, which are occupied by the accumulating species themselves over time. The temperature plays a role in this process and the highest accumulation rate is found at 200 °C (Fig. S3†). Carbon contaminations formed on the surface during the exposure to carbon dioxide hydrogenation reaction conditions (C_xH_y) react with hydrogen and yield methane at high temperature (around 400 °C), as shown by the TPR experiment in Fig. 1d. Because the accumulation of carbon-species is much slower in nitrogen and pure carbon dioxide (Fig. S4 and S5†), these cannot originate exclusively from impurities in the reaction cell but are significantly influenced by the gas phase. In particular, the addition of hydrogen favours the accumulation of carbon; this is assumed to be promoted by hydrodeoxygenation of oxygen-containing species (adsorbed CO_2), yielding unreactive, oxygen-free carbon species accumulating on the surface. Hydrogenation of C–O bonds[21] and the C–O bond breaking[22] can already start around 100 °C on specific catalysts, and might take place also on silver at a very low reaction rate, covering the surface over 60–120 min. Fig. S1† shows that no hydroxyls accumulate on the surface in parallel to carbon, while water desorption is detected in the TPR experiment (Fig. S9†). This suggests that any oxygen splitting off from carbon dioxide reacts to form water at a much higher reaction rate than the hydrodeoxygenation, which then desorbs from the surface.

The STM images combine the spectroscopic information with a microscopic characterization of the metal surface before and after exposure to the reaction environment. While there are studies where the silver deposition on mica substrate leads to a highly ordered Ag(111) surface,[23] the sample investigated in this study rather suggests disordered silver. This is indicated by the corrugations in the apparent step height in Fig. 2a, smaller than 2.36 Å, which corresponds to the atomic step height of Ag(111), and a very faint low energy electron diffraction (LEED) pattern of the surface (Fig. S15†). The step edges observable on the clean silver surface exposed to high-temperature conditions appear mobile (Fig. S6†), as already reported for other silver surfaces.[24,25] Conversely, the sample exposed to the H_2 + CO_2 mixture at 1 mbar and 200 °C (Fig. 2b and S8†) shows flat terraces intersected by rather defined step edges. The step edges appear oftentimes with a clear border and decorated by protrusions, which can be reversibly removed after repeating the high-temperature treatment. Knowing that the carbon species observed by AP-XPS accumulates over the course of 60–120 min at low temperatures and shows the same temperature dependency, we tentatively assign them to the protrusions observed by STM. Since the step edges are coordinatively unsaturated sites on metal surfaces, they can bind stronger to surface species compared to the pristine metal surface. Depending on the relation between step edge stability and particle adsorption strength, the step edge can be denoted as "pinned"[26,27] (fixation of mobile step edges at fixed adsorbate) or "decorated"[28–30] (fixation of mobile adsorbates at fixed step edges). For example, it was observed that adsorbed oxygen (O_{ad}) can pin silver step edges.[31] For several materials, it is observed that mobile carbon deposits accumulate along step edges.[10,32] In the case of nickel, known for its high activity towards methanation of carbon dioxide and thus more intensely studied,[33] disproportionation or dissociation of carbon dioxide on the surface and especially on atomic nickel steps can even lead to the formation of carbon nanotubes or whiskers.[33,34] It is also demonstrated that atomic carbon at

step edges is the active species for methane formation.[35] These literature works, combined with AP-XPS and STM data in this study, indicate that the strong increase in the sharpness of step edges is due to the pinning of adsorbed C_xH_y (hydro-) carbon species. The presence of hydrogen in the accumulating species can neither be detected by XPS nor STM, thus y in C_xH_y could also be zero.

A different situation is observed upon the deposition of zinc oxide nanoparticles on the silver surface. For both high- and low-temperature exposure, no step edges with the characteristic protrusions or pinned step edges are observed (Fig. 3 and Fig. S11–S14†). Step edges imaged by STM rather resemble those observed on unexposed, clean silver. If migration of zinc atoms onto or into the silver surface takes place under these conditions, such as observed on ZnO/Cu,[36] could not be resolved.

AP-XPS measurements on the high surface area ZnO/Ag sample (Fig. 4) show a peak centered at 289.7 eV, which can be assigned to zinc carbonate.[37,38] The species appears immediately after the first contact with gas phase carbon dioxide and decreases in intensity during exposure to reaction conditions. In the opposing trend, a species creating the signal at 285.5 eV builds up over 90 min of exposure. The position of the peak is shifted by 1 eV compared to the main C 1s peak component observed on clean silver, suggesting a reduced electron density on carbon. Considering the availability of C, O and H elements from the educt gases, we assign this species to oxygen-containing carbon species adsorbed on the silver surface ($C_xH_yO_z$). Felter *et al.* assign an adsorbed methoxy species on silver to a signal at 285.0 eV,[39] Zugic *et al.* assign a signal at 285.7 eV to C–O species on Ag/Au.[40]

The ZnO/Ag system shows the transient formation of carbonates (Fig. 4) and should be active towards the RWGS reaction (producing carbon monoxide and water) even at 1 mbar total pressure according to thermodynamics. We assign these carbonates to form on the zinc oxide, they can then be reduced by adsorbed hydrogen at the interface between silver and zinc oxide. This leads to the generation of an oxygen source, which on silver influences the chemical composition of surface adsorbates and, hereby, also the silver surface structure. A similar effect has been observed for platinum on alumina, where the oxygen spillover from the platinum allows coke burning on the alumina substrate,[41] and even the effect of an oxygen-providing catalyst over 50 μm separated from the soot has been observed.[42]

In the absence of zinc oxide, this chemisorption and reaction of carbon dioxide will probably only take place on surface defects with coordinatively unsaturated sites. After this chemisorption, adsorbed hydrogen on the silver can fully hydrodeoxygenate the adsorbed species.

Conclusions

This study, combining the investigation of different model systems, shows that the surface of a working catalyst depends on the applied temperature, the gas environment, the presence of co-catalysts, and the reaction time. In situ XPS reveals the accumulation of oxygen-free (hydro-)carbon species C_xH_y on the surface of silver upon exposure to a reactive environment (CO_2 + H_2, 1 : 3 ratio, 200 °C). STM images acquired upon exposure to the same reaction environment show protrusions on the silver step edges, which are tentatively assigned to these carbonaceous species. Adsorption of species on metal step edges can poison these often catalytically active sites and significantly influence the materials' macroscopic activity. While the accumulation shows the highest rate at 200 °C, it suddenly drops to zero at 350 °C, also removing all present carbon adsorbates and lifting the pinning of step edges.

The deposition of zinc oxide nanoparticles, thus the creation of catalytically active metal/oxide interfaces, favours the formation of oxygenated carbon species, $C_xH_yO_z$. This chemical change of the surface adsorbate strongly influences the appearance of the silver surface, as no step edge pinning is observed. The influence of zinc oxide on the surface structure of silver proves the synergy between metal and oxide in bifunctional catalytic materials. This synergy is not limited to reaction intermediates but influences the presence of all adsorbates. For catalytic reactions where the oxidic phase is not required for the reaction mechanism itself, it could still increase the catalyst lifetime by enhancing the intrinsic regeneration of the metal.

Concerning the development of low-temperature carbon dioxide hydrogenation catalysts, our results show that not only the general activity of the catalyst towards the desired reaction is important, but also the material regeneration to counteract poisoning of active sites. In this study, the silver-based catalyst is only regenerating above 350 °C in the reaction environment. The potential presence of such a sudden temperature-dependent transition in surface morphology should be considered for catalyst design and the choice of operational conditions.

Methods

AP-XPS experiments were performed at the In Situ Spectroscopy (ISS) beamline of the Swiss Light Source (SLS) synchrotron facility.[43] Polycrystalline silver foil (Thermo Fisher, 99.998%) was pretreated by plasma cleaning cycles in oxidative (O_2 + Ar) and reducing (H_2 + He) plasma. After insertion into the measurement chamber, the sample was heated in the reaction mixture (0.2 mbar H_2 (Linde, purity 5.0) + CO_2 (Linde, purity 4.5) 3 : 1 mixture) to 350–450 °C to remove any remaining impurities. From this reference condition, the sample temperature was lowered to the respective measurement temperatures in less than 1 min. Spectra were acquired at 437 eV (C 1s), 520 eV (Ag 3d) and 684 eV (O 1s) photon energies, to probe core level peaks at the same kinetic energy of 150 eV (same information depth). Linearly polarized light was used throughout the experiments. The spectra were referenced to the Ag 3d signal acquired at equal photon energy (Fig. S16†). The photon flux was determined by measurement of the current on

a photodiode inserted in the beam path. Photoelectrons were detected using a differentially pumped Scienta R4000 HiPP-2 electron energy analyzer coupled to an MCP/CCD camera. An IR-laser (976 nm wavelength) was focused on the sample holder from the back to heat the sample.

The high surface area ZnO/Ag catalyst was synthesized by co-precipitation. $Ag(NO_3)$ and $Zn(NO_3)_2 \times 6\ H_2O$ were dissolved in water, acidified to pH 5 and dropwise added to an aqueous solution of Na_2CO_3 + HNO_3 at pH 8.5 at 65 °C. Aqueous Na_2CO_3 solution (1 M) was added in parallel to maintain a pH value of 8.5, leading to the precipitation of the metal carbonates. The precipitate was filtered and washed thoroughly with water, then dried for 60 min at 75 °C. Calcination in air was performed by a heating ramp of 120 min to 350 °C followed by 5 h at constant temperature and a subsequent cooling to room temperature. XRD spectra show separate phases for Ag (domains >60 nm) and ZnO (domains ≈22 nm) and are displayed in Fig. S17.† ICP measurements show a 1 : 1 atomic ratio for Ag : Zn, BET measurements indicate a surface area of 21 $m^2\ g^{-1}$ (Fig. S18†). Further characterization of the ZnO/Ag catalyst can be found in a separate publication.[13]

Scanning tunneling microscopy (STM) and low energy electron diffraction (LEED) measurements were performed at room temperature in a vacuum chamber with a base pressure of 2×10^{-9} mbar. STM images were acquired using an Omicron variable-temperature (VT-)STM operated by R9Plus electronics (RHK Technology). Exposure to reactive conditions was performed inside the vacuum system in an enclosed high-pressure cell with a base pressure of 3×10^{-7} mbar. Acquired images were analyzed using the Gwyddion software[44] (version 2.64). Measurement conditions are summarized in Table S2.†

The silver substrates used for STM measurements were thin films (200 nm) magnetron-sputtered on mica substrates using an intermediate 5 nm chromium adhesion layer. The films were annealed to 350 °C in 1×10^{-6} mbar O_2 for 70 min followed by the same temperature treatment in ultra-high vacuum overnight. Zinc oxide nanoparticles were deposited on the silver thin films in high vacuum environment using a pulsed microplasma cluster source described in detail in ref. 45. The size and distribution of the nanoparticles was determined by atomic force microscopy (AFM), details shown in Fig. S10.†

The samples annealed in the vacuum chamber for STM measurements were exposed to 1 mbar H_2 + CO_2 (3 : 1) mixture. The samples annealed at 200 °C were first annealed to 375 °C for 5 min (heating rate 2 °C s^{-1}) to receive a clean surface, before lowering the temperature to 200 °C and keeping it for 60 min. The samples annealed to high temperature were heated to 350 °C for 60 min and after this, the temperature was increased to 375 °C for a further 5 min, before cooling the sample to room temperature.

Hydrogen temperature-programmed reaction (H_2-TPR) was done by using a silver powder to increase the sample surface area. The powder was synthesized by titration of $Ag(NO_3)$ with Na_2CO_3, followed by drying at 110 °C overnight. The sample cleanliness was checked by XPS (Fig. S19†). 100 mg Ag powder were loaded in a quartz tube reactor degassed at 900 °C, heated in He gas to 250 °C, then exposed to H_2 for 10 min before switching to CO_2 gas. After 5 min, the sample was heated to 400 °C (10 °C min^{-1}), and kept for 5 min at 400 °C. It is known from AP-XPS that these conditions lead to very clean silver surfaces. Then the temperature was lowered to 200 °C, the reaction mixture (3 : 1 H_2 + $^{12}CO_2$) was introduced and kept for 30 min. After this exposure, the temperature was lowered to 50 °C, CO_2 was switched off and a temperature ramp (20 °C min^{-1}) to 600 °C was performed in a flow of pure hydrogen while measuring the released gases with a mass spectrometer (Pfeiffer Omnistar).

Author contributions

P. M. L.: Conceptualization, data curation, investigation, funding acquisition, writing – original draft. M. P.: Investigation. V. L. S.: Investigation. P. P.: Investigation. A. P.: Investigation. J. A. v. B.: Project administration, supervision. L. A.: Funding acquisition, supervision. All authors: Writing – review & editing.

Data availability

Data supporting this article have been included as part of the ESI.† Raw STM images (.sm4 format) and the XPS spectra displayed in the main manuscript (.csv format) have been uploaded to the following data repository: **https://doi.org/10.5281/zenodo.14268803**.

Conflicts of interest

There are no conflicts to declare.

Acknowledgements

The authors thank Dr Jeffrey Brock for the preparation of the Ag/mica samples, Man Guo for beamtime support and Stefano Vigneri for support in the STM measurements. This project has received funding from the European Union's Horizon 2020 research and innovation programme under grant agreement no 101007417 having benefited from the access provided by CNR-IOM in Trieste and UMIL in Milano within the framework of the NFFA-Europe Pilot Transnational Access Activity, proposal ID456. The authors acknowledge the Swiss Light Source (SLS) for the provision of beamtime at the X07DB (In Situ Spectroscopy) beamline.

References

1 J. H. K. Pfisterer, Y. Liang, O. Schneider and A. S. Bandarenka, Direct instrumental identification of cat-

alytically active surface sites, *Nature*, 2017, **549**, 74–77, DOI: 10.1038/nature23661.
2 B. Böller, K. M. Durner and J. Wintterlin, The active sites of a working Fischer–Tropsch catalyst revealed by operando scanning tunnelling microscopy, *Nat. Catal.*, 2019, **2**, 1027–1034, DOI: 10.1038/s41929-019-0360-1.
3 K. Roy, L. Artiglia and J. A. van Bokhoven, Ambient Pressure Photoelectron Spectroscopy: Opportunities in Catalysis from Solids to Liquids and Introducing Time Resolution, *ChemCatChem*, 2018, **10**, 666–682, DOI: 10.1002/cctc.201701522.
4 M. Zabilskiy, *et al.*, The unique interplay between copper and zinc during catalytic carbon dioxide hydrogenation to methanol, *Nat. Commun.*, 2020, **11**, 2409, DOI: 10.1038/s41467-020-16342-1.
5 H. Yang, *et al.*, Predictions of Chemical Shifts for Reactive Intermediates in CO2 Reduction under Operando Conditions, *ACS Appl. Mater. Interfaces*, 2021, **13**, 31554–31560, DOI: 10.1021/acsami.1c02909.
6 M. Behrens, *et al.*, The active site of methanol synthesis over Cu/ZnO/Al_2O_3 industrial catalysts, *Science*, 2012, **336**, 893–897, DOI: 10.1126/science.1219831.
7 B. Mockenhaupt, *et al.*, High-Pressure Pulsing of Ammonia Results in Carbamate as Strongly Inhibiting Adsorbate of Methanol Synthesis over Cu/ZnO/Al_2O_3, *J. Phys. Chem. C*, 2023, **127**, 3497–3505, DOI: 10.1021/acs.jpcc.2c08823.
8 J. Abu-Dahrieh, D. Rooney, A. Goguet and Y. Saih, Activity and deactivation studies for direct dimethyl ether synthesis using CuO–ZnO–Al_2O_3 with NH4ZSM-5, HZSM-5 or γ-Al_2O_3, *Chem. Eng. J.*, 2012, **203**, 201–211, DOI: 10.1016/j.cej.2012.07.011.
9 B. Eren, *et al.*, Activation of Cu(111) surface by decomposition into nanoclusters driven by CO adsorption, *Science*, 2016, **351**, 475–478, DOI: 10.1126/science.aad8868.
10 S. Helveg, *et al.*, Atomic-scale imaging of carbon nanofibre growth, *Nature*, 2004, **427**, 426–429, DOI: 10.1038/nature02278.
11 J. Zhou, *et al.*, Regeneration of catalysts deactivated by coke deposition: A review, *Chin. J. Catal.*, 2020, **41**, 1048–1061, DOI: 10.1016/s1872-2067(20)63552-5.
12 S. A. Theofanidis, R. Batchu, V. V. Galvita, H. Poelman and G. B. Marin, Carbon gasification from Fe–Ni catalysts after methane dry reforming, *Appl. Catal., B*, 2016, **185**, 42–55, DOI: 10.1016/j.apcatb.2015.12.006.
13 P. M. Leidinger, *et al.*, Influence of alumina on the performance of Ag/ZnO based catalysts for carbon dioxide hydrogenation, *J. Catal.*, 2024, **440**, 115837, DOI: 10.1016/j.jcat.2024.115837.
14 M. Bowker, Methanol Synthesis from CO(2) Hydrogenation, *ChemCatChem*, 2019, **11**, 4238–4246, DOI: 10.1002/cctc.201900401.
15 K.-J. Lee, Y. Ye, H. Su, B. S. Mun and E. J. Crumlin, Correlating the Reverse Water–Gas Shift Reaction with Surface Chemistry: The Influence of Reactant Gas Exposure to Ni(100), *ACS Catal.*, 2023, **13**, 9041–9050, DOI: 10.1021/acscatal.3c01517.
16 A. Beck, M. A. Newton, L. G. A. van de Water and J. A. van Bokhoven, The Enigma of Methanol Synthesis by Cu/ZnO/Al(2)O(3)-Based Catalysts, *Chem. Rev.*, 2024, **124**, 4543–4678, DOI: 10.1021/acs.chemrev.3c00148.
17 K. Christmann, in *Surface and Interface Science*, 2016, pp. 255–356.
18 J. Hohmeyer, *et al.*, Activation of dihydrogen on supported and unsupported silver catalysts, *J. Catal.*, 2010, **269**, 5–14, DOI: 10.1016/j.jcat.2009.10.008.
19 X. Chen, X. Wang and D. Fang, A review on C1s XPS-spectra for some kinds of carbon materials, *Fullerenes, Nanotubes Carbon Nanostruct.*, 2020, **28**, 1048–1058, DOI: 10.1080/1536383x.2020.1794851.
20 C. E. Taylor, S. D. Garvey and J. E. Pemberton, Carbon Contamination at Silver Surfaces: Surface Preparation Procedures Evaluated by Raman Spectroscopy and X-ray Photoelectron Spectroscopy, *Anal. Chem.*, 1996, **68**, 2401–2408, DOI: 10.1021/ac950753h.
21 S. Kim, *et al.*, Recent advances in hydrodeoxygenation of biomass-derived oxygenates over heterogeneous catalysts, *Green Chem.*, 2019, **21**, 3715–3743, DOI: 10.1039/c9gc01210a.
22 A. Beuls, *et al.*, Methanation of CO2: Further insight into the mechanism over Rh/γ-Al_2O_3 catalyst, *Appl. Catal., B*, 2012, **113–114**, 2–10, DOI: 10.1016/j.apcatb.2011.02.033.
23 D.-A. Luh, *et al.*, Single-crystalline silver films on mica, *Thin Solid Films*, 2018, **645**, 215–221, DOI: 10.1016/j.tsf.2017.10.051.
24 M. Poensgen, J. F. Wolf, J. Frohn, M. Giesen and H. Ibach, Step dynamics on Ag(111) and Cu(100) surfaces, *Surf. Sci.*, 1992, **274**, 430–440, DOI: 10.1016/0039-6028(92)90848-z.
25 H.-C. Jeong and E. D. Williams, Steps on surfaces: experiment and theory, *Surf. Sci. Rep.*, 1999, **34**, 171–294, DOI: 10.1016/s0167-5729(98)00010-7.
26 J. S. Ozcomert, W. W. Pai, N. C. Bartelt and I. E. Reutt-Robey, Step configurations near pinning sites on Ag(110), *Surf. Sci.*, 1993, **293**, 183–194, DOI: 10.1016/0039-6028(93)90312-8.
27 F. Behafarid and B. R. Cuenya, Nano Pinstripes: TiO2 Nanostripe Formation by Nanoparticle-Mediated Pinning of Step Edges, *J. Phys. Chem. Lett.*, 2012, **3**, 608–612, DOI: 10.1021/jz300022c.
28 C. L. Aravinda, I. Mukhopadhyay and W. Freyland, Electrochemical in situ STM study of Al and Ti–Al alloy electrodeposition on Au(111) from a room temperature molten salt electrolyte, *Phys. Chem. Chem. Phys.*, 2004, **6**, 5225–5231, DOI: 10.1039/b407846m.
29 F. Abild-Pedersen, *et al.*, Methane activation on Ni(111): Effects of poisons and step defects, *Surf. Sci.*, 2005, **590**, 127–137, DOI: 10.1016/j.susc.2005.05.057.
30 M.-F. Hsieh, H.-D. Li, D.-S. Lin and K. Morgenstern, Formation, Binding, and Stability of O-Ag-CO2-Ag-O Compounds on Ag(100) Investigated by Low Temperature Scanning Tunneling Microscopy and Manipulation, *J. Phys. Chem. C*, 2010, **114**, 14173–14179, DOI: 10.1021/jp104170b.

31 J. K. Plischke and M. Albert Vannice, Effect of pretreatment on the adsorption properties of silver crystallites, *Appl. Catal.*, 1988, **42**, 255–283, DOI: **10.1016/0166-9834(88)80007-1**.
32 J. K. Nørskov, *et al.*, Universality in Heterogeneous Catalysis, *J. Catal.*, 2002, **209**, 275–278, DOI: **10.1006/jcat.2002.3615**.
33 I. Czekaj, *et al.*, Characterization of surface processes at the Ni-based catalyst during the methanation of biomass-derived synthesis gas: X-ray photoelectron spectroscopy (XPS), *Appl. Catal., A*, 2007, **329**, 68–78, DOI: **10.1016/j.apcata.2007.06.027**.
34 S. Helveg, J. Sehested and J. R. Rostrup-Nielsen, Whisker carbon in perspective, *Catal. Today*, 2011, **178**, 42–46, DOI: **10.1016/j.cattod.2011.06.023**.
35 B. Miao, S. S. K. Ma, X. Wang, H. Su and S. H. Chan, Catalysis mechanisms of CO2 and CO methanation, *Catal. Sci. Technol.*, 2016, **6**, 4048–4058, DOI: **10.1039/c6cy00478d**.
36 S. Jensen, *et al.*, Visualizing the gas-sensitive structure of the CuZn surface in methanol synthesis catalysis, *Nat. Commun.*, 2024, **15**, 3865, DOI: **10.1038/s41467-024-48168-6**.
37 T. Koitaya, *et al.*, CO2 Activation and Reaction on Zn-Deposited Cu Surfaces Studied by Ambient-Pressure X-ray Photoelectron Spectroscopy, *ACS Catal.*, 2019, **9**, 4539–4550, DOI: **10.1021/acscatal.9b00041**.
38 C. T. Au, W. Hirsch and W. Hirschwald, Adsorption of carbon monoxide and carbon dioxide on annealed and defect zinc oxide (000) surfaces studied by photoelectron spectroscopy (XPS and UPS), *Surf. Sci.*, 1988, **197**, 391–401, DOI: **10.1016/0039-6028(88)90635-8**.
39 T. E. Felter, *et al.*, The adsorption of methanol on Ag(111) and its reaction with preadsorbed oxygen, *Appl. Surf. Sci.*, 1983, **16**, 351–364, DOI: **10.1016/0378-5963(83)90079-x**.
40 B. Zugic, *et al.*, Evolution of steady-state material properties during catalysis: Oxidative coupling of methanol over nanoporous Ag0.03Au0.97, *J. Catal.*, 2019, **380**, 366–374, DOI: **10.1016/j.jcat.2019.08.041**.
41 E. Baumgarten and A. Schuck, Oxygen spillover and its possible role in coke burning, *Appl. Catal.*, 1988, **37**, 247–257, DOI: **10.1016/s0166-9834(00)80764-2**.
42 K. Yamazaki, Y. Sakakibara, F. Dong and H. Shinjoh, The remote oxidation of soot separated by ash deposits via silver–ceria composite catalysts, *Appl. Catal., A*, 2014, **476**, 113–120, DOI: **10.1016/j.apcata.2014.02.014**.
43 F. Orlando, *et al.*, The Environmental Photochemistry of Oxide Surfaces and the Nature of Frozen Salt Solutions: A New in Situ XPS Approach, *Top. Catal.*, 2016, **59**, 591–604, DOI: **10.1007/s11244-015-0515-5**.
44 D. Nečas and P. Klapetek, Gwyddion: an open-source software for SPM data analysis, *Open Phys.*, 2012, **10**, 181–188, DOI: **10.2478/s11534-011-0096-2**.
45 E. Barborini, P. Piseri and P. Milani, A pulsed microplasma source of high intensity supersonic carbon cluster beams, *J. Phys. D: Appl. Phys.*, 1999, **32**, L105–L109, DOI: **10.1088/0022-3727/32/21/102**.